Thermochimica Acta 473 (2008) 86–91

Contents lists available at ScienceDirect

Thermochimica Acta

journal homepage: www.elsevier.com/locate/tca

Correlation between thermal properties and hardness of end-quench bars for C48, 42CrMo4 and 35NiCrMo16 steels

Taher Ghrib*, Fatah Bejaoui, Abdelwahheb Hamdi, Noureddine Yacoubi

Photothermal Laboratory, I PEI 8000 Nabeul, Tunisia

ARTICLE INFO

Article history:
Received 24 July 2007
Received in revised form 31 March 2008
Accepted 4 April 2008
Available online 23 April 2008

Keywords:
End-quench bars
Steel
Hardness
Thermal conductivity
Thermal diffusivity
Photothermal deflection

ABSTRACT

The thermal properties, the Rockwell hardness (HRC) and the microstructure of three end-quench bar (Jominy bar) steels (C48, 42CrMo4 and 35NiCrMo16) have been investigated. The thermal properties are determined using photothermal deflection (PTD) technique and the hardness is measured by the Rockwell durometer. In this paper we have tried to relate the thermal properties to the hardness for each steel illustrated by an empiric mathematical equation.

1. Introduction

The use of the heat treatment to improve hardness and the resistance of alloys goes back to moved back times [1,2]. As the determination of the mechanical properties uses generally destructive methods such as (hardness, elasticity, stress, tenacity, ...), it is preferable to relate the mechanical properties to other kinds of physical properties in which determination is easy and to use non-destructive techniques such as the law of Petch which relates the grain size to the elasticity constant R_e: [3] $R_e = R_e + \beta/\sqrt{d}$ where R_e is edge elasticity, β is a constant that depends on materials and d is grain diameter.

Photothermal deflection (PTD) technique [4–12] which is a non-destructive technique is widely used for carrying out the thermal and optical properties of materials [7–12].

In this work we have used the PTD [4,5,10,12] in order to determine the thermal conductivity and thermal diffusivity of steel having undergone a heat treatment in volume (Jominy tests) [13–15]. We have investigated the thermal properties and hardness variation along the Jominy bar and tried to relate them by using an empiric equation.

2. Heat treatment and preparation of the sample

The Jominy sample (Fig. 1) is a cylindrical bar of a diameter 25.4 mm and length 100 mm provided with a flat part of width 2 mm along its length. The treatment consists of heating the sample at a temperature superior to the austenitization one (850 °C) for about 30 min. After the austenitization operation the sample is quickly taken from the furnace and placed vertically on a standardized water jet of temperature 12 °C to be cooled starting from the lower extremity for at least 15 min, however the other extremity is cooled in ambient air at a temperature of 18 °C.

This test was carried out on three steels of nuances C48, 42CrMo4 and 35NiCrMo16 which composition are given on Table 1. Also thermal and hardness measurements are done on the bar surface. As the hardness and thermal properties determination need a flat surface, the sample may undergo a polishing operation to eliminate the oxide layer.

To study the sample micrograph, it is necessary to carry out a chemical attack of smoothed surface by a reagent composed of (HNO_3 (4%) + ethanol) which will highlight the grains morphology.

3. Determination of the thermal properties

3.1. Theoretical model (Fig. 2)

The PTD method [4,12] consists of heating one sample using a modulated light pump beam. As the hardened steel sample has a

* Corresponding author. Fax: +216 72 220 181.
E-mail address: taher.ghrib@yahoo.fr (T. Ghrib).

0040-6031/$ – see front matter © 2008 Elsevier B.V. All rights reserved.
doi:10.1016/j.tca.2008.04.008

Table 1
Massic composition of the C48, 42CrMo4 and 35NiCrMo16 used steel

Massic composition	C (%)	Mn (%)	Si (%)	S (%)	P (%)	Ni (%)	Cr (%)	Mo (%)	Cu (%)
C48	0.5	0.67	0.24	0.022	0.031				
42CrMo4	0.44	0.8	0.31	0.013	0.03	0.46	0.96	0.05	0.18
35NiCrMo16	0.34	0.36	0.26	0.006	0.008	3.55	1.54	0.31	0.008

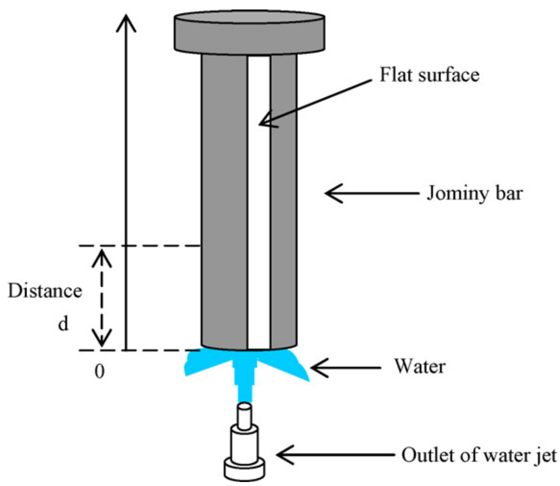

Fig. 1. Soak Jominy test-tube.

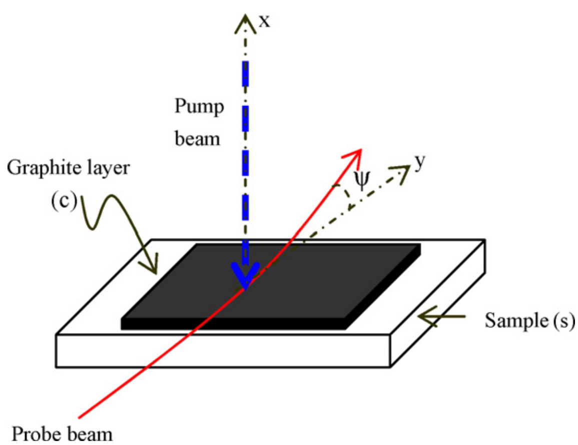

Fig. 2. Principle of the photothermal deflection techniques.

great reflection coefficient the flat sample surface should be covered with a thin graphite layer that will absorb the incident light and therefore serve as a heat source. The optical absorption of the sample will generate a thermal wave that will propagate into the sample and in the surrounding fluid medium, inducing a temperature gradient and then a refractive index gradient in the fluid. A Laser probe beam that skims the sample surface and crosses the region with inhomogeneous refractive index gradient is deflected. Its deflection ψ may be related to the thermal properties of the sample, the fluid and the backing. In the case of a uniform heating of the sample, a one-dimensional treatment of the thermal wave is sufficient and the signal deflection is given by [12]:

$$\psi = |\psi| e^{j(\omega t+\varphi)} = \frac{\sqrt{2}l}{n\mu_f}\frac{dn}{dT_f}|T_0| e^{(-x/\mu_f)} e^{j(\theta+(5\pi/4)-(x/\mu_f))} e^{j\omega t} \quad (1)$$

where T_0 is the surface temperature rise given by [12]:

$$T_0 = \frac{E[(1-b)e^{-\sigma_s l_s}[(1-r)(1-c)e^{\sigma_c l_c}+(1+r)(1+c)e^{-\sigma_c l_c}-2(1+rc)e^{-\alpha l_c}]-(1+b)e^{\sigma_s l_s}[(1-r)(1+c)e^{\sigma_c l_c}+(1+r)(1-c)e^{-\sigma_c l_c}-2(1-rc)e^{-\alpha l_c}]]}{[[(1+b)e^{\sigma_s l_s}[(1+g)(1+c)e^{\sigma_c l_c}+(1-g)(1-c)e^{-\sigma_c l_c}]-(1-b)e^{-\sigma_s l_s}[(1+g)(1-c)e^{\sigma_c l_c}+(1-g)(1+c)e^{-\sigma_c l_c}]]} \quad (2)$$

$$b = \frac{K_b}{K_s}\sqrt{\frac{D_s}{D_b}}, \quad c = \frac{K_c}{K_s}\sqrt{\frac{D_s}{D_c}}, \quad g = \frac{K_f}{K_c}\sqrt{\frac{D_c}{D_f}},$$

$$r = \frac{(1-j)\alpha}{2\mu_c}, \quad \sigma_i = (1+j)\sqrt{\frac{\pi f}{D_i}}$$

K_i, D_i, and μ_i are respectively the thermal conductivity, the thermal diffusivity and the thermal diffusion length of the i medium (f, c, s, b) designating the fluid as 'f', the black graphite layer as 'c', the sample as 's' and the backing as 'b'.

$$|\psi| = \frac{\sqrt{2}l}{n\mu_f}\frac{dn}{dT_f}|T_0| e^{-x/\mu_f} \quad (3a)$$

And

$$\varphi = -\frac{x}{\mu_f} + \theta + \frac{5\pi}{4} \quad (3b)$$

Are the theoretical signal amplitude and phase of the probe beam deflection and $|T_0|$, θ are respectively the amplitude and phase of the sample's surface temperature.

3.2. Experimental set-up

The experimental set-up (Fig. 3) which is described in detail in Ref. [12], is composed with a halogen heating lamp, a laser probe beam, a photodetector position and a look-in amplifier. The light coming from the halogen lamp is modulated by a mechanical chopper. The sample is fixed on an *xy* table improving micrometric displacement. A laser prop beam skimming the sample surface is deflected. Its deflection is measured by a position photodetector sensor.

3.3. Experimental results

3.3.1. Determination of the thermal properties

In order to determine the thermal properties of the Jominy bar along its length, we have to study the variation of the photothermal signal with the square root of the modulation frequency for different values of *d* (*d* is the distance between the quenched extremity and the measurement point).

The curves of Fig. 4 represent the amplitude and phase variations with the square root modulation frequency for three values of d (3 mm, 15 mm and 60 mm) for the C48 steel. We note from these curves that the signal varies with *d* i.e. the thermal properties vary along the Jominy bar. The best theoretical fitting curves are obtained for fixed values K_s and D_s [12].

Table 2 gives the experimental obtained values of thermal conductivity and thermal diffusivity for the three steels according to the distance *d*.

If we draw the experimental variations of both thermal conductivity and thermal diffusivity with the *d* distance, we can notice from the curves of Fig. 5 that the two thermal properties increase with the distance *d* respectively for the C48 and 42CrMo4 soaked steel until a distance of 50 mm and remain constant after this

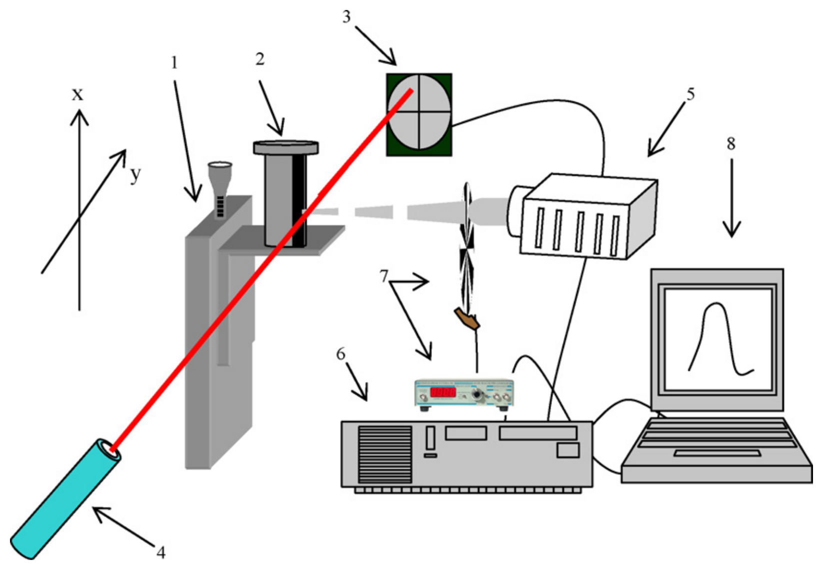

Fig. 3. Experimental set-up: (1) table of horizontal and vertical micrometric displacement, (2) sample, (3) position photodetector, (4) fixed laser source, (5) halogen Lamp, (6) look-in amplifier, (7) mecanical chopper, (8) PC.

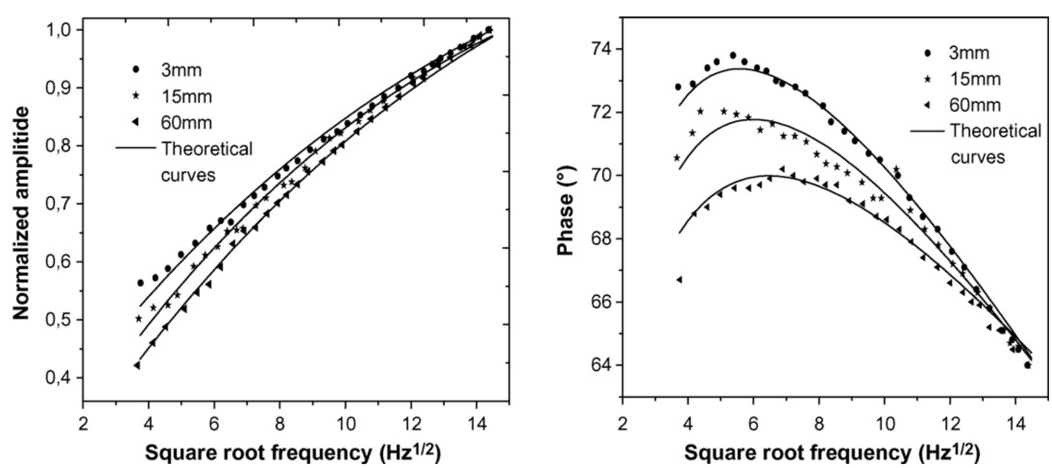

Fig. 4. Experimental and theoretical amplitude and phase variation according to the square root modulation frequency for the standard Jominy bar of C48 steel at the positions d = 3 mm, 15 mm and 60 mm.

Table 2
Experimental values of thermal conductivity and thermal diffusivity of C48, 42CrMo4 and 35NiCrMo16 Jominy bar for different d values

	XC48		42CD4		35NCD16	
Distance d (mm)	Thermal conductivity ($W\,m^{-1}\,K^{-1}$)	Thermal diffusivity ($10^{-4}\,m^2\,s^{-1}$)	Thermal conductivity ($W\,m^{-1}\,K^{-1}$)	Thermal diffusivity ($10^{-4}\,m^2\,s^{-1}$)	Thermal conductivity ($W\,m^{-1}\,K^{-1}$)	Thermal diffusivity ($10^{-4}\,m^2\,s^{-1}$)
3	29	0.1	29	0.09	28	0.1
5	30	0.11	29	0.11	28	0.11
7	31.5	0.11	29.5	0.12	29	0.1
9	33	0.11	29.5	0.13	29	0.1
11	35	0.12	30	0.135	29	0.1
13	36	0.14	31	0.138	30	0.11
15	37	0.16	33	0.14	30	0.11
20	43	0.18	36	0.15	29	0.11
30	46	0.19	38	0.16	29	0.1
40	50	0.2	42	0.17	30	0.1
50	54	0.21	47	0.18	31	0.11
60	56	0.22	49	0.19	30	0.1
70	55	0.22	49	0.18	30	0.1
80	56	0.22	49	0.19	31	0.11

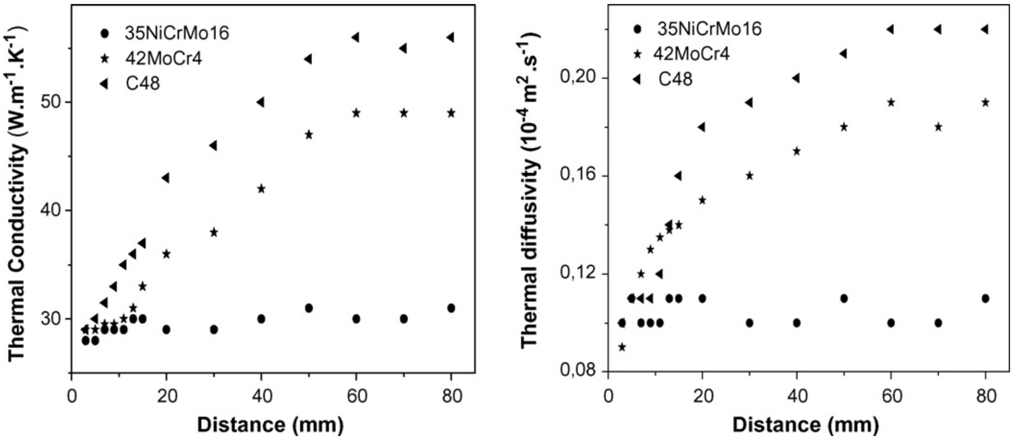

Fig. 5. Experimental thermal diffusivity and thermal conductivity variation with the distance *d* for the three samples C48, 42CrMo4, 35NiCrMo16.

distance. However one can notice that for the 35NiCrMo16 the thermal properties are independent of the distance *d*. This variation of the thermal properties may be related to the rate of alloys so we can observe a high variation for the C48 which is non-allied steel, a lower variation for the 42CrMo4 which is lower allied steel and finally no variation for the 35NiCrMo16 which is high allied steel.

3.3.2. Measurements of Rockwell hardness (HRC)

Using a durometer we carried out the measurement of Rockwell hardness of the three tubes at the same positions used to determine the thermal properties.

The curves of Fig. 6 show the hardness variations with the distance *d* for the three samples.

According to these curves, one can notice that the mechanical hardness decreases gradually from the soaked extremity until a distance *d* of about 50 mm respectively for steels C48, 42CrMo4 and remains constant for the 35NiCrMo16 steel.

These variations of the thermal and mechanical properties are primarily related to the various microstructures of the samples which are given by the micrographics photo of Figs. 7–10 for a magnification of 1000.

For steel 35NiCrMo16 the micrographics photo shows that the sample has the same structure in the entire bar given by Fig. 7 which demonstrates according to the CCT diagram that the structure is composed with 50% of bainite and 50% of martensite.

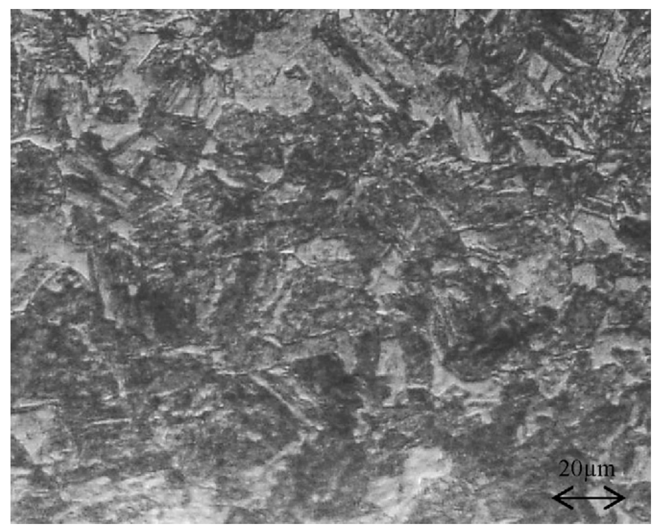

Fig. 7. Microstructure of 35NiCrMo16 Jominy bar along the surface for a magnification of 1000.

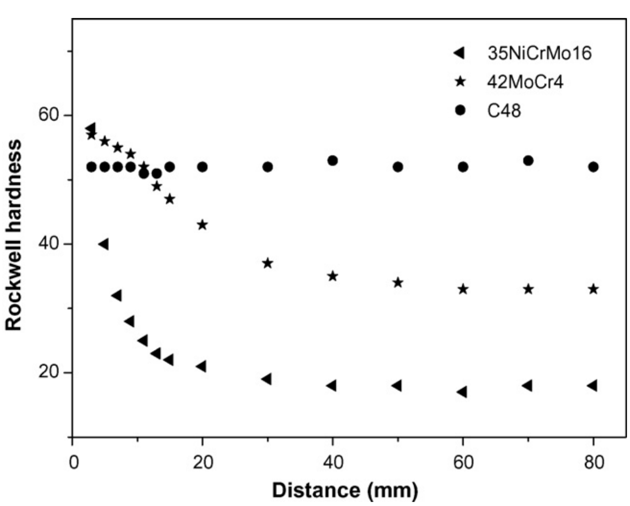

Fig. 6. Rockwell hardness evolution with the distance *d* for the three samples C48, 42CrMo4, 35NiCrMo16.

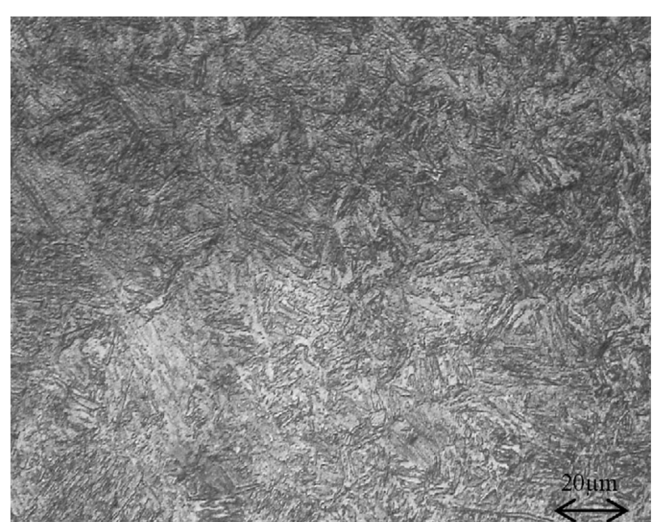

Fig. 8. Microstructure of C48 and 42CrMo4 for *d* = 3 mm for a magnification of 1000.

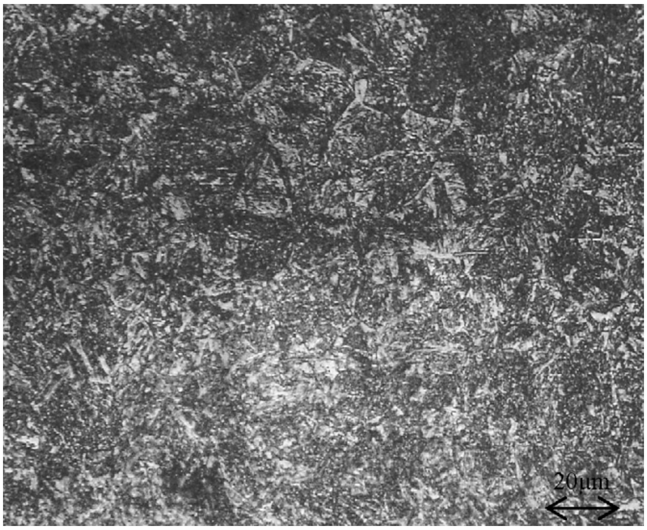

Fig. 9. Microstructure of steel to 42CrMo4 for $d = 40$ mm and $d = 70$ mm for a magnification of 1000.

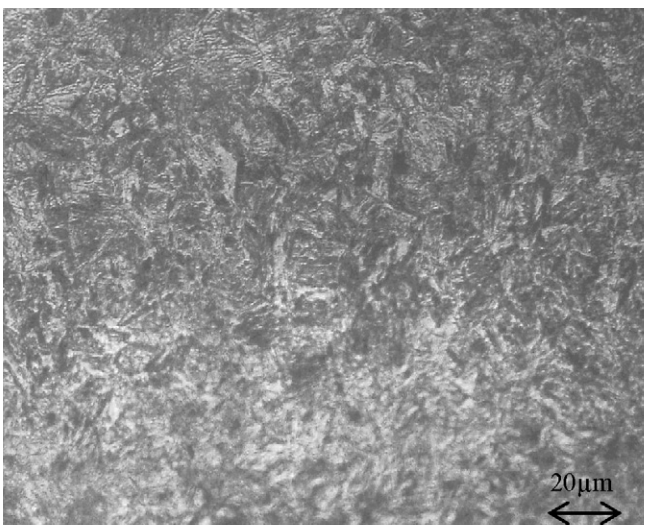

Fig. 10. Microstructure of steel to C48 for 40 mm and 70 mm for a magnification of 1000.

Table 3
Values of the coefficients A, A', B, B', C and C'

	C48	42CrMo4	35NiCrMo16
A ($K\,s\,m^{-2}$)	2.151	2.234	1.766
A' ($10^4\,J\,s\,m^3$)	588.067	598.060	502
B ($K\,s\,m^{-3}$)	−0.006	0.024	0
B' ($10^4\,J\,s\,m^2$)	2.463	1.064	0
C ($m^3\,K^{-1}\,s^{-1}$)	0.025	0.129	0
C' ($10^4\,J^{-1}\,s^{-1}\,m^{-4}$)	0.132	0.043	0

Whereas for the 42CrMo4 and the C48 steel, the micrographic structure of Figs. 8–10 taken respectively at the distances $d = 3$ mm, 40 mm and 70 mm for the two steel one can notice a structure change. Indeed at the distance $d = 3$ mm the structure is purely Martensitic (100% of Martensite) for the two steel (Fig. 8). For $d = 40$ mm and $d = 70$ mm the structure is composed according to the CCT diagram of 15% of Ferrite, 20% of Perlite, 40% of Bainite and 25% of Martensite for the 42CrMo4 steel (Fig. 9). However for steel C48, micrographies of Figs. 8 and 10 show a change in the structure from the Martensite structure (100% Martensite) at the soaked extremity (Fig. 8) to a structure composed of 60% of Perlite and 40% of Ferrite at the other extremity (Fig. 10).

3.3.3. Correlation between thermal and mechanical properties

Fournier and coworkers [8] have studied the steel 18CrMo5 thermically treated at the surface, measured the Vickers hardness and determined thermal conductivity by the conventional method using a stationary heat flow and the thermal diffusivity by using the photothermal microscope. Their study permits them to affect to each hardness value the corresponding thermal conductivity and thermal diffusivity.

In this work we have projected to relate the thermal properties to hardness by drawing the variations of the ratios hardness/thermal conductivity and hardness/thermal diffusivity according to the distance d for the three kinds of steel. The obtained curves are shown on Fig. 11. One can notice that the obtained curves obey to the same empirical law given by the equations:

$$\frac{\mathrm{HRC}}{K_s} = \frac{A + B.d}{1 + C.d} \quad \text{and} \quad \frac{\mathrm{HRC}}{D_s} = \frac{A' + B'.\mathrm{d}}{1 + C'.\mathrm{d}}$$

where A, A', B, B', C and C' are constant and changes only with the nature of the studied steel. Table 3 gives the values of A, A', B, B', C and C' for the three steels.

So for a known steel if we have the value of the thermal conductivity or the thermal diffusivity at a fixed distance d, one can

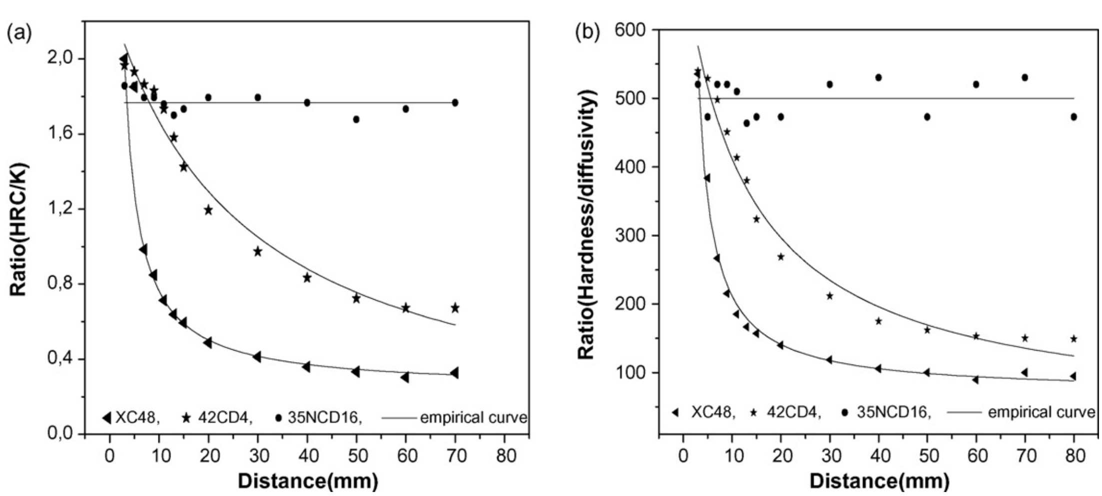

Fig. 11. Variation of ratios hardness–thermal conductivity and hardness–thermal diffusivity with the distance d (mm) for the three samples C48, 42CrMo4 and 35NiCrMo16.

determine the hardness of the steel at this position without needing to measure it.

4. Conclusion

In this work, we have investigated the thermal properties and the Rockwell hardness for three end-quench bars and we have noticed that their variations are related to the microstructural change. We have shown that for 42CrMo4 and C48 steels the thermal properties and the hardness vary with the distance *d* but remain steady for the 35NiCrMo16 steel. The correlation between the thermal properties and the hardness is illustrated by an empirical mathematical law that allows us to determine the hardness value at a fixed position of the Jominy bar without needing to measure it if we know the thermal conductivity or the thermal diffusivity at this point.

References

[1] Ferchault de Réaumur, "L'art de convertir le fer forgé en acier et l'art d'adoucir le fer fondu" book, Paris, 1722, editor: Michel Brunet.
[2] J. Fariaut, C. Boulmer-Leborgne, et al., Surf. Coat. Technol. 6–147 (2001) 324–330.
[3] C.E. Carlton, P.J. Ferreira, Acta Mater. 55 (2007) 3749–3756.
[4] N. Yacoubi, H. Mani, Photoacoustic and Photothermal, Phenomena II, 62, Springer series in optical sciences, Heidelberg, 1990, pp. 173–177.
[5] P.K. Kuo, M.J. Lin, C.B. Reyes, L.D. Favro, R.L. Thomas, D.S. Kim, Shu-YI. Zhang, L.J. Inglehart, D. Fournier, A.C. Boccara, L.J. Inglehart, N. Yacoubi, Part I: experiment, Can. J. Phys. 64 (1986) 1168–1175.
[6] A. Salazar, A. Sanchez-lavega, J. Fernandez, J. Appl. Phys. 69 (1991) 1216–1223.
[7] J. Bodzenta, B. Burak, W. Hofman, M. Gala, J. Kucytowski, T. Lukasiewicz, M. Pyka, K. Wokulska, J. de Physique IV france 117 (2004) 7–12.
[8] H.G. Walther, D.Fournier, J. C. Krapez, M. Luukkala, B. Schmitz, C. Sibilia, H. Stamm, J. Thoen, The Japan Society for Analytical Chemistry, vol. 17, special issue, 2001, pp. 165–168.
[9] A. Balderas-Lopez, A. Mandelis, J.A. Garcıa, Appl. Phys. 92 (6) (2002) 3047–3055.
[10] F. Saadallah, N. Yacoubi, F. Genty, C. Alibert, J. Appl. Phys. 41 (8) (2003) 7561–7568.
[11] J. Kauppinen, K. Wilcken, I. Kauppinen, V. Koskinen, J. Microchem. 76 (2004) 151–159.
[12] Taher Ghrib, Noureddine Yacoubi, Faycel Saadallah, J. Sens. Actuators A 135 (2007) 346–354.
[13] Standard method for end-quench test for hardenability of steel ASTM designation A 255–Annual Book of ASTM Standards, ASTM, 1989, pp. 27–44.
[14] K. Yamanaka, Y. Ohmori, Trans. ISIJ 18 (1978) 404–411.
[15] M. Larsson, B. Jansson, R. Blom, A. Melander, Scand. J. Metall. 19 (1990) 51–63.